A&A 442, 841–849 (2005)
DOI: 10.1051/0004-6361:20053433

Astronomy & Astrophysics

New spectroscopic confirmations of high-redshift galaxy clusters⋆,⋆⋆

L. F. Olsen[1,2], E. Zucca[3], S. Bardelli[3], C. Benoist[1], L. da Costa[4,5], H. E. Jørgensen[2], A. Biviano[6], and M. Ramella[6]

[1] Observatoire de la Côte d'Azur, Laboratoire Cassiopée, BP 4229, 06304 Nice Cedex 4, France
[2] Niels Bohr Institute, Copenhagen University, Juliane Maries Vej 30, 2100 Copenhagen, Denmark
e-mail: lisbeth@astro.ku.dk
[3] INAF - Osservatorio Astronomico di Bologna, via Ranzani 1, 40127 Bologna, Italy
[4] Observatorio Nacional, Rua General Jose Cristinino 77, CEP 20921-400, Rio de Janeiro JR, Brazil
[5] European Southern Observatory, Karl-Schwartzschild-Str. 2, 85748 Garching b. München, Germany
[6] INAF - Osservatorio Astronomico di Trieste, Via G.B. Tiepolo 11, 34131 Trieste, Italy

Received 13 May 2005 / Accepted 21 July 2005

ABSTRACT

We present new spectroscopic data in the field of five high-redshift ($z \geq 0.6$) candidate galaxy clusters, drawn from the EIS Cluster Candidate Catalog. A total of 327 spectra were obtained using FORS1 at the VLT, out of which 266 are galaxies with secure redshifts. In this paper, we use these data for confirming the existence of overdensities in redshift space at the approximate same location as the matched-filter detections in the projected distribution of galaxies from the EIS *I*-band imaging survey. The spectroscopic redshifts, associated to these overdensities, are consistent but, in general, somewhat lower than those predicted by the matched-filter technique. Combining the systems presented here with those analyzed earlier, we have spectroscopically confirmed a total of nine overdensities in the redshift range $0.6 < z < 1.3$, providing an important first step in building an optically-selected, high-redshift sample for more detailed studies, complementing those based on the few available X-ray selected systems.

Key words. cosmology: observations – galaxies: distances and redshifts – galaxies: clusters: general

1. Introduction

Clusters of galaxies are large bound systems that evolve from large-scale fluctuations, making their existence at large redshifts an important constraint on cosmological models. They are also ideal sites to study galaxy evolution, once systems at different redshifts are available. Combined, these characteristics have stimulated systematic searches for large, statistical samples of galaxy clusters at large redshifts ($z \gtrsim 0.5$). With few exceptions most of the systems identified, especially those at very large redshifts, have been serendipitous discoveries in deep X-ray exposures. While this work has provided confirmation for the existence of these systems, only a handful of clusters have been identified.

A more promising alternative is to use moderately deep, optical or near-infrared surveys to search for concentrations in the projected galaxy distribution as originally carried out by Postman et al. (1996) and later used by Olsen et al. (1999a,b) and Scodeggio et al. (1999), among others. While finding cluster candidates using these single-passband imaging surveys is much easier and yields much larger samples than using the available X-ray data, the task of confirming that the systems correspond to true density enhancements in redshift space and going even further to bound systems is much harder.

Over the past few years our group has been engaged in an effort to study galaxy systems at different redshift ranges with the aim of confirming and if possible determining the nature of the EIS cluster candidates (Olsen et al. 1999a,b; Scodeggio et al. 1999). Previous work have included Olsen et al. (2003, 2005) for systems at low redshift ($z \lesssim 0.4$), and Ramella et al. (2000) for systems at intermediate redshifts ($0.5 \lesssim z \lesssim 0.7$). For candidates with estimated redshifts larger than $z \gtrsim 0.6$ we have carried out observations with FORS1 and FORS2 mounted at the VLT. Preliminary results were presented by Benoist et al. (2002) who showed strong evidence for a system at $z = 1.3$. The present paper extends these earlier results by presenting the result of VLT spectroscopic observations of 5 additional fields.

In Sect. 2 we discuss how the candidate clusters were selected from the original catalog and how available photometric data were used to select individual galaxy targets, aiming

⋆ Based on observations collected at the European Southern Observatory, Chile under the programs ESO65.O-0192(B) and ESO65.O-0189(A).

⋆⋆ Tables A1–A5 are only available in electronic form at http://www.edpsciences.org

Table 1. Basic properties for the targeted candidate clusters. The parameters are described in the text and more details can be found in Olsen et al. (1999a).

EIS cluster	α (J2000)	δ (J2000)	$z_{\rm MF}$	$\Lambda_{\rm cl}$	N_R	$I-K_{\rm s}$	$J-K_{\rm s}$
EISJ0046-2951	00:46:07.4	−29:51:44.5	0.9	157.0	2	2.75	1.75
EISJ0048-2942	00:48:31.6	−29:42:52.1	0.6	55.6	13	2.75	1.75
EISJ0050-2941	00:50:04.4	−29:41:35.6	1.0	175.3	62	3.50	1.60
EISJ2236-4017	22:36:18.0	−40:17:54.9	0.6	107.8	47	2.90	1.45
EISJ2249-3958	22:49:33.0	−39:58:10.1	0.9	123.6	29	2.75	1.90

at improving the efficiency of the observations by eliminating foreground and background objects. In Sect. 3 the observations and data reduction are summarized. In Sect. 4 the results of the spectroscopic observations are presented for each of the fields considered. In Sect. 5 these results are combined with those of Benoist et al. (2002) to draw conclusions regarding the efficiency of the matched-filter technique applied to moderately deep I-band survey data in building a statistical sample of high-redshift galaxy clusters. Finally, in Sect. 6, the main results of the present paper are summarized.

2. Sample selection

Cluster candidates were drawn from the sample of EIS cluster candidates compiled by Olsen et al. (1999a,b) and Scodeggio et al. (1999) applying the matched-filter technique to the EIS-WIDE I-band imaging survey covering 17 square degrees. The eight target clusters, of which three were discussed by Benoist et al. (2002), were selected based on their identification as likely clusters in a color slice analysis (Olsen 2000). This analysis was based on the optical survey data combined with infrared follow-up imaging. Based on the fact that most clusters exhibit a red sequence of early-type galaxies (e.g. Gladders et al. 1998; Stanford et al. 1998) we searched for concentrations of galaxies with similar color by separating the galaxies in slices of color and identifying peaks in the density distribution for each color. The analysis was carried out separately for the $I-K_{\rm s}$ and $J-K_{\rm s}$ colors. The systems selected for follow-up spectroscopy all appeared to have significant overdensities in both $I-K_{\rm s}$ and $J-K_{\rm s}$. In Table 1 we present the detection information, both for the matched filter and the color slicing, regarding the five candidates discussed in this work. The table gives: in Col. 1 the field name; in Cols. 2 and 3 the nominal position of the cluster candidate in J2000; in Col. 4 the redshift estimated by the matched-filter algorithm; in Col. 5 the $\Lambda_{\rm cl}$-richness, which measures the equivalent number of L^* galaxies and in Col. 6 the Abell like richness giving the number of galaxies in the magnitude interval $[m_3; m_3+2]$, where m_3 is the third brightest galaxy. For both richnesses more details can be found in Olsen et al. (1999a); in Cols. 7 and 8 the $I-K_{\rm s}$ and $J-K_{\rm s}$-colors obtained from the color-slicing analysis. When comparing the computed colors of the cluster galaxies to those expected for a passively evolving elliptical galaxy we find that in general, the $I-K_{\rm s}$-colors are bluer, while the $J-K_{\rm s}$-colors were found to be roughly consistent with these expectations. This may be caused by a poor calibration of the IR data used for the preliminary analysis.

The selection of target galaxies in each field was based on a combination of data from as many bands as available. For the candidates EISJ0046-2951, EISJ0048-2942, EISJ0050-2941 we derived photometric redshifts based on $BVIJK_{\rm s}$ imaging. The limiting magnitude used for this work was $I=22.5$ to avoid large errors in the derived photometric redshifts. The primary targets were selected among galaxies with $z_{\rm phot}\geq 0.5$ (∼50% of the target galaxies). Remaining slits were filled with arbitrarily chosen objects. For the targets selected to have $z_{\rm phot}\geq 0.5$ ∼ 70% proved to have a spectroscopic redshift $z_{\rm spec}\geq 0.5$. A more thorough discussion of the photometric redshifts is the topic of a forthcoming paper.

For the clusters EISJ2236-4017 and EIS2249-3958 only $IJK_{\rm s}$ imaging data were available at the time of the spectroscopic observations. For these clusters we selected galaxies based on their optical-infrared colors to match those of elliptical galaxies at $z\geq 0.5$. Remaining slits were filled with arbitrarily chosen galaxies.

3. Observations and data reduction

The observations were carried out in the nights September 21–25, 2000, using FORS1 mounted at the VLT-ANTU telescope. We used the multi-object spectroscopy (MOS) mode, in which FORS1 provides 21 slits with lengths of 20 and 22 arcsecs (see the FORS Manual for details). The length of the slits is much longer than necessary for each galaxy, thus as often as possible we tried to fit two galaxies in the slits. In practice, however, this was rarely possible. The MOS masks were positioned using the FIMS-software developed for this purpose. We used the I-band images from the ESO Imaging Survey (Nonino et al. 1999; Benoist et al. 1999) to determine the positions of the slits. We used grism 150I+17 with the order separation filter OG590 covering the wavelength range 6000–11 000 Å. The dispersion of 230 Å/mm corresponding to 5.52 Å/pixel gave a spectral resolution of 280 or about 29 Å for a slit width of 1.4 arcsecs. The exposure times for each mask were either 60 min or 120 min, depending on the I-band magnitude of the target galaxies. We split the exposures into four or eight 15 min exposures. Calibration frames (flatfields and calibration arcs) were obtained during daytime.

We reduced the spectra using IRAF-tasks written for this purpose based on the APALL task. Details on the reduction procedure and measurement of redshift are available in Jørgensen et al. (2005, in preparation). Here, it suffices to say that the individual science exposures were combined and a flatfield correction applied before the wavelength calibration.

Table 2. The identified groups with significance $\sigma \geq 99\%$.

Cluster	α (J2000)	δ (J2000)	# galaxies	z	σ_v (km s^{-1})	Significance
EIS0046-2951	00:46:04.2	−29:49:27.6	17	0.614	1400^{+210}_{-610}	99.9
EIS0046-2951	00:46:07.7	−29:51:04.9	10	0.671	865^{+120}_{-270}	99.7
EIS0048-2942	00:48:35.4	−29:41:52.4	7	0.402	1000^{+100}_{-480}	99.4
EIS0048-2942	00:48:33.4	−29:42:28.9	33	0.637	1080^{+150}_{-210}	>99.9
EIS0050-2941	00:50:06.2	−29:40:35.3	12	0.558	1375^{+190}_{-270}	99.9
EIS0050-2941	00:50:03.0	−29:40:18.1	8	0.616	970^{+210}_{-620}	99.1
EIS2236-4017	22:36:22.0	−40:17:55.0	12	0.509	900^{+160}_{-260}	99.9
EIS2249-3958	22:49:32.1	−39:58:02.9	8	0.710	380^{+50}_{-140}	99.4

Redshifts were computed by cross-correlating the extracted one-dimensional spectra against template spectra, taken from Kinney et al. (1996), properly shifted to a redshift close to that expected for the galaxy being measured as estimated from features in the galaxy spectrum. We apply this procedure iteratively, and also for different galaxy spectra. Before a redshift was accepted it was compared with the presence of corresponding spectral features. The redshifts derived in this way are listed in Tables A.1–A.5. We estimate an accuracy of the individual redshifts of $\delta z = 0.0004 \sim 130$ km s^{-1}. In these tables a value of 8.8888 indicates that the spectrum revealed a stellar object.

4. Results

We have secured a total of 266 new galaxy redshifts. The distribution of the redshifts of each field is shown in the upper panels of Fig. 1. These panels give in their upper parts a bar diagram of all the measured redshifts and in their lower parts the distribution of redshifts (dashed line) with the solid line indicating identified groups as discussed below. The figure also shows for each field the redshifts versus right ascension and declination respectively (lower panels, left and right).

As in previous papers of this series, we use the "gap"-technique originally proposed by Katgert et al. (1996) for identifying groups in redshift space. We adopt a gap-size of 0.005(1+z) to separate individual groups. This separation corresponds to a restframe velocity of 1500 km s^{-1}. In addition, only systems with a group redshift $z > 0.4$ and with at least 3 galaxies are considered for further analysis. This lower limit on the redshift corresponds to an offset from the original matched-filter estimate of $\Delta z = 0.2$ which should be sufficient to include all confirmations.

To assess the significance of each group we have used simulated data sets based on the expected redshift distribution for a uniform distribution of galaxies with a given luminosity function (LF). The redshift distribution is built for the same limiting magnitude as was used for the target selection ($I = 22.5$). It was confirmed that this approach leads to a redshift distribution which is consistent with that measured by the Canada-France Redshift Survey (Lilly et al. 1995) when the same limiting magnitude is adopted (for further details see Benoist et al. 2002). We determine the significance of the detected groups from the probability of finding a group as rich or richer at the same redshift. To do this we draw 1000 sets of galaxies from the redshift distribution constructed above, with the size given by the number of redshifts measured in each of the cluster fields. We select only galaxies with $z \geq 0.4$ to mimic the color pre-selection of our targeted galaxies. For each set we run our group finding method to obtain the frequency of groups as rich or richer than and at the same redshift (within $\Delta z \leq 0.05$) as the group detected in the spectroscopic data. This constraint in redshift is necessary because, due to the shape of the selection function, the frequency of groups with a certain number of members varies with redshift. The significance of the group is defined to be $1-f$, where f is the redshift dependent frequency.

Applying the gap-technique to the redshift distributions shown in Fig. 1, and adopting the same criteria used in previous papers to consider only density enhancements with a significance ≥99%, we identify 8 groups. Their properties are summarized in Table 2 which gives: in Col. 1 the name of the EIS cluster field; in Cols. 2 and 3 the J2000 right ascension and declination; in Col. 4 the number of member galaxies; in Col. 5 the redshift of the group; in Col. 6 its biweight estimated rest-frame velocity dispersion corrected for our measurement accuracy with 68% bootstrap errors; and finally, in Col. 7 the significance, as defined above. The positions given in the table are mean values computed using the spectroscopically confirmed member galaxies. Below the detections for each individual cluster field are briefly discussed using the available color information to provide additional information.

4.1. EISJ0046-2951

In this field 71 galaxy redshifts have been measured and are shown in Fig. 1. We identify 6 groups with at least 3 members at $z \geq 0.4$, out of which only 2, one at $z = 0.614$ and the other at $z = 0.671$ have significance ≥ 99% and are, therefore, included in Table 2.

In order to decide which of these groups is the one most likely associated with the matched-filter detection we examined both the cone diagrams (Fig. 1) and the projected distribution of the galaxies with redshifts as shown in Fig. 2. In the cone diagrams the foreground system is more prominent than the background one, due to its larger extent. From the projected distribution of the galaxies, it is clear that the center of the foreground group deviates significantly from that of the matched-filter algorithm, located at the center of the field.

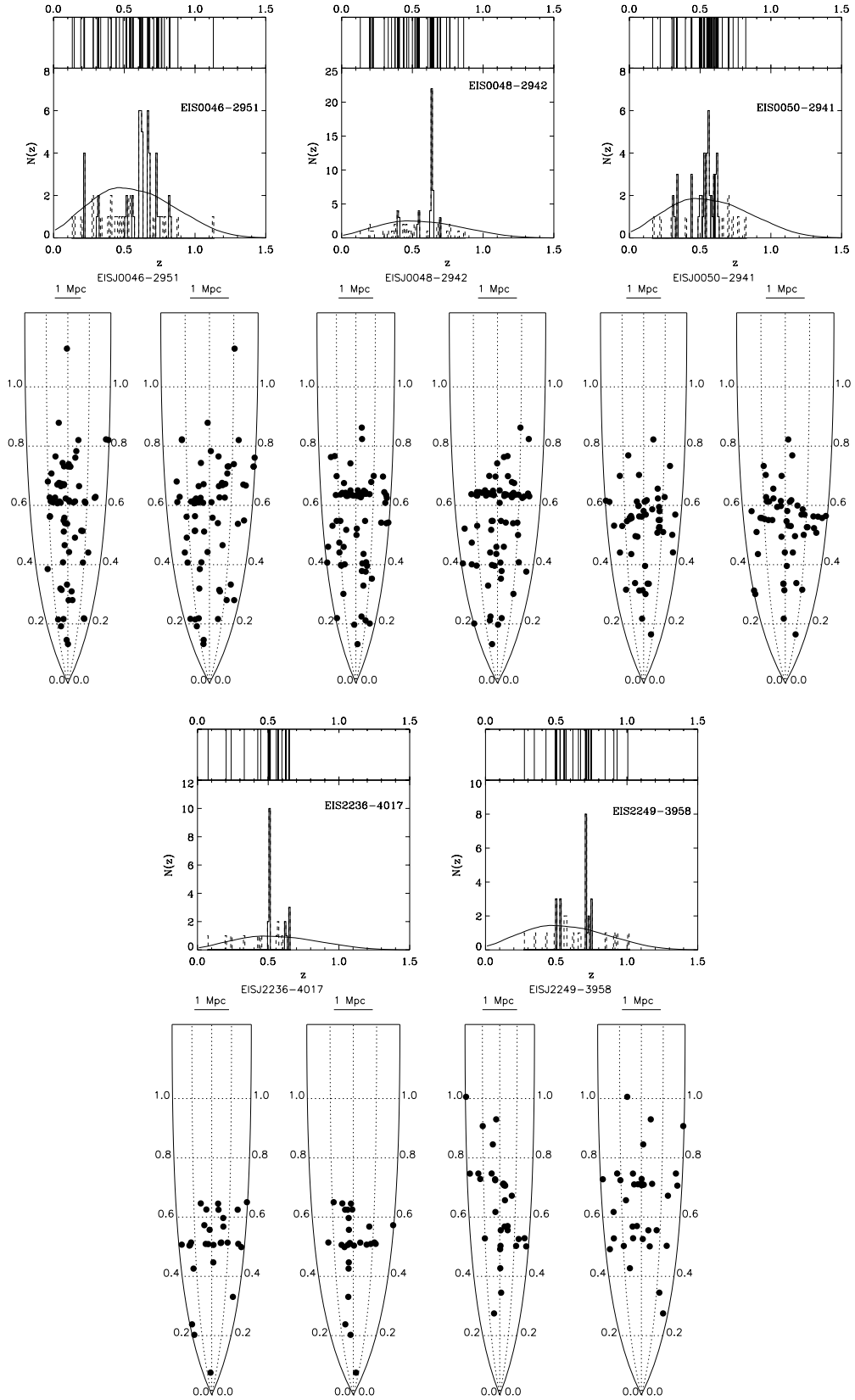

Fig. 1. For each cluster the obtained redshifts (*upper panels*) and the redshifts as function of right ascension and declination (*lower panels, left and right*) are shown. In the upper panel the upper part gives a bar diagram of the redshifts, while the lower part gives the redshift distribution (dashed line) with the identified groups (solid line). In the lower panels the left cone shows the redshifts as function of right ascension and the right one the redshifts as function of declination. The diagrams correspond to the complete coverage of each field. The bar in the top of each cone gives the scale of 1 h_{75}^{-1} Mpc The shape of the cones translates the evolution of scale with redshift.

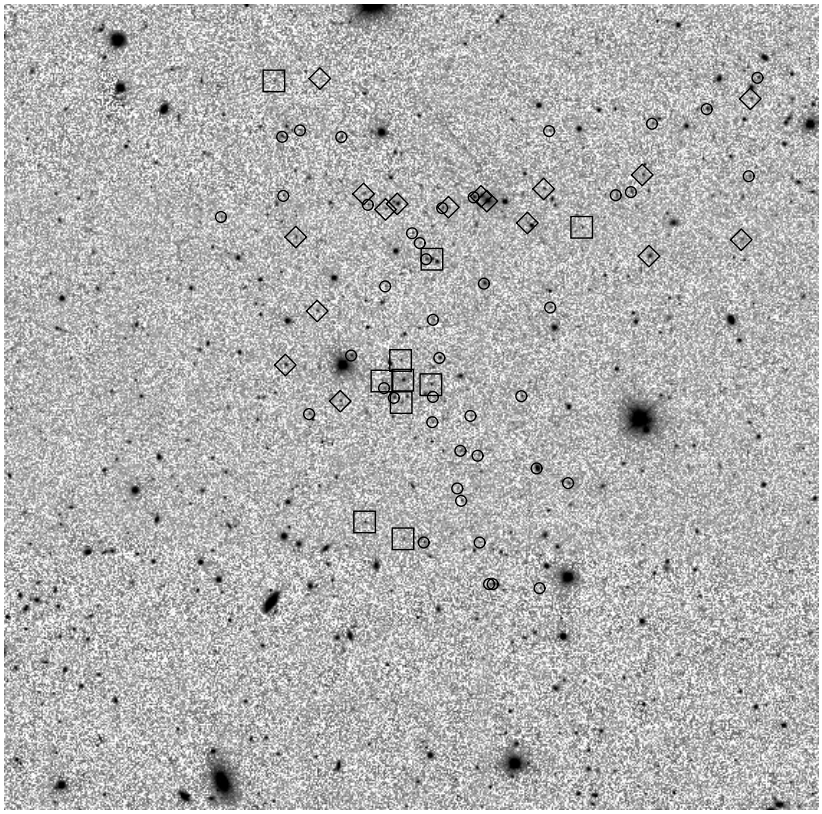

Fig. 2. A 10×10 arcmin cutout centered on the matched-filter position of EISJ0046-2951. The circles mark galaxies with redshifts outside significant groups. The diamonds mark galaxies in the foreground group and the squares those in the background group. North is up, east to the left.

The background group, on the other hand, consists of 10 members out of which five form a compact system located very close to the center derived by the matched filter and five more uniformly distributed. Furthermore, from the examination of the image one finds that the five galaxies situated near the center are also among the brightest galaxies in the central region. It should also be kept in mind that the radial part of the matched filter gives a significantly higher weight to galaxies close to the estimated position, thus the galaxies closest to the originally estimated position are the ones contributing the most, even when other systems are found at almost the same redshift and in the same field. Combined these arguments suggest that the background group at $z = 0.671$ ($\Delta z = z_{\rm spec} - z_{\rm MF} \sim -0.23$) and with an estimated velocity dispersion of $\sigma_v = 865\,{\rm km\,s^{-1}}$ is the most likely to correspond to the EIS cluster candidate identified by the matched-filter algorithm, with the difference between the estimated and measured redshifts being consistent with the expected errors. Another possible explanation, could be that the matched-filter detection at a larger redshift is correct but system galaxies have not been observed or had no measured redshifts. However, careful inspection of the image show no evidence for any further clustering of faint galaxies in the field.

4.2. EISJ0048-2942

The distribution of the 77 redshifts measured in this field is presented in Fig. 1. As it can be seen, the distribution shows a distinct spike around $z \sim 0.6$, in excellent agreeement with the value estimated by the matched filter. The gap-technique identifies 3 groups with at least 3 members in this field, out of which two have significance ≥99% and are therefore included in Table 2 – one with seven members at $z = 0.402$ and a more prominent background group with 33 members at $z = 0.637$.

The examination of the redshift distribution and the cone diagrams for this cluster (shown in Fig. 1) leaves little doubt that the background concentration at $z = 0.638$ ($\Delta z \sim 0.04$) corresponds to the matched-filter detection, with cluster galaxies being distributed over nearly the entire field. This conclusion is also supported by the image of the field shown in Fig. 3. The velocity dispersion of this system is estimated to be $\sigma_v = 1080\,{\rm km\,s^{-1}}$ indicating a massive system.

Combined, the photometric (color and projected distribution) and spectroscopic results provide strong evidence that we have detected a real galaxy cluster at a redshift in excellent agreement with that estimated by the matched-filter algorithm.

4.3. EISJ0050-2941

In this field 55 redshifts have been measured and are shown in the last panel in the first row of Fig. 1. The distribution is considerably more complex than in the previous case, with no single dominant peak discernible. The gap-technique identifies 6 groups with at least 3 members in the field, out of which two, with comparable number of members, satisfy our significance criterion. Information about these two systems is given in Table 2 – a foreground system with 12 members at

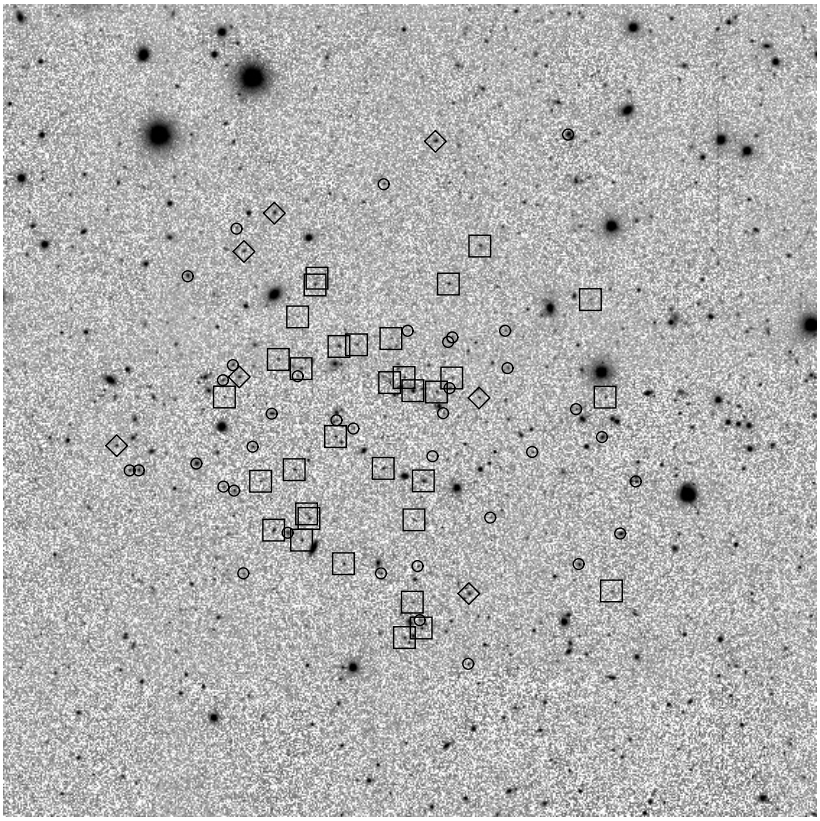

Fig. 3. A 10×10 arcmin cutout centered on the matched-filter position of EISJ0048-2942. Symbols follow those in Fig. 2. North is up, east is to the left.

$z = 0.558$ and a more distant background system with 8 members at $z = 0.616$. Note that both systems are at considerably smaller redshifts than that estimated by the matched filter and their projected spatial distribution (see Fig. 4) is scattered over the entire field. Taken together this casts some doubt on the association of these density enhancements in redshift space with the matched-filter detection at $z_{\rm MF} = 0.9$. In addition, the colors listed in Table 1 point to a more distant concentration. These colors correspond to the reddest of two peaks detected by the color-slicing analysis by Olsen (2000). The identification of two color peaks indicate the presence of two superposed systems of which one is possibly more distant than indicated by the spectroscopic redshifts.

In order to investigate this point further, we visually examined the available imaging data (Fig. 4), finding an apparent clustering of faint galaxies very close to the position of the matched-filter detection but only two of these galaxies have a measured redshift (with $z \sim 0.39$ and $z \sim 0.58$). Still there are many more faint galaxies in the concentration and it is conceivable that a more distant system may still exist lying behind two widely scattered foreground systems. It is unclear at the present time whether the matched-filter detection corresponds to the combination of the two spectroscopically identified systems, with the faint galaxies leading to an overestimate of the matched-filter redshift, or whether the original detection is caused by a background concentration without measured redshifts and the two identified systems lying in the foreground. Clearly, with the available data alone it is not possible to resolve this ambiguity which must await additional spectroscopic observations in the field.

Regardless of the interpretation, the present results strongly suggest the presence of two systems with estimated velocity dispersions of 1375 and 970 $\mathrm{km\,s^{-1}}$ for the foreground and background systems, respectively, but with redshift offsets about twice as large as the estimated accuracy.

4.4. EISJ2236-4017

In this field 28 redshifts were measured and are shown in the left panel in the second row of Fig. 1. As in the case of EISJ0048-2942 the redshift distribution shows a distinct peak at $z \sim 0.5$ as well as the suggestion of other enhancements at somewhat larger redshifts (e.g., $z \sim 0.65$). In fact, the gap-technique identifies 3 groups with at least 3 members in the field. However, only one satisfies our significance criterion. The properties of this system are given in Table 2. It has 12 members and a redshift of 0.509 which, even though slightly smaller, is consistent with that estimated by both the matched-filter and the color-slicing technique. A cutout of the cluster region with field and member galaxies marked is shown in Fig. 5. The system does not appear to be very concentrated but has member galaxies being uniformly distributed, even though the color slicing showed a strong peak at the position of the matched-filter detection (Olsen 2000). However, for this field

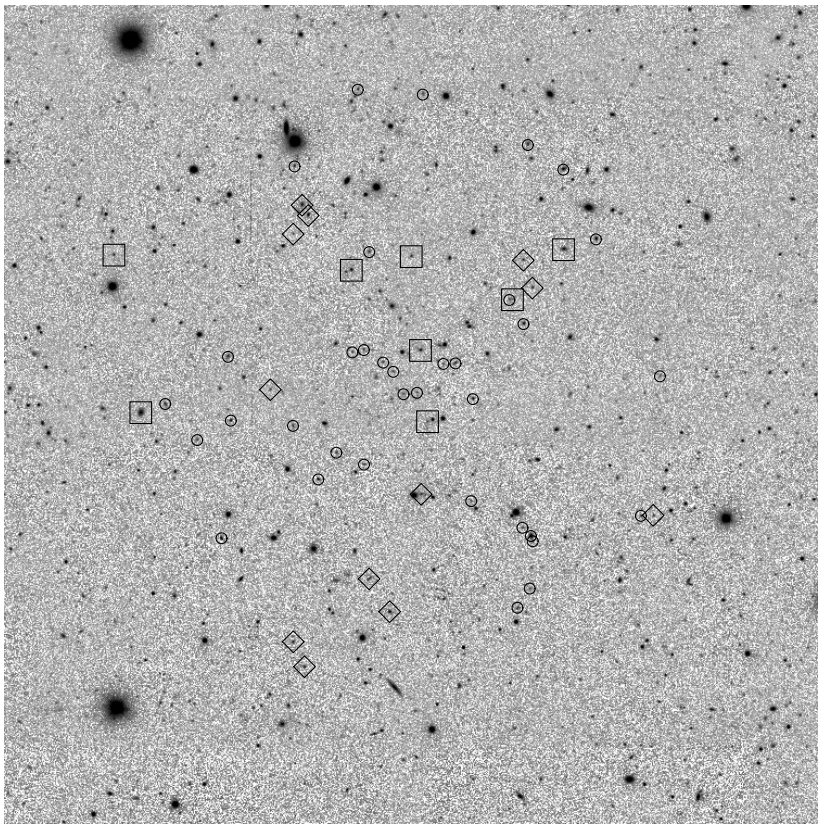

Fig. 4. A 10 × 10 arcmin cutout centered on the matched-filter position of EISJ0050-2941. Symbols follow those in Fig. 2. North is up, east to the left.

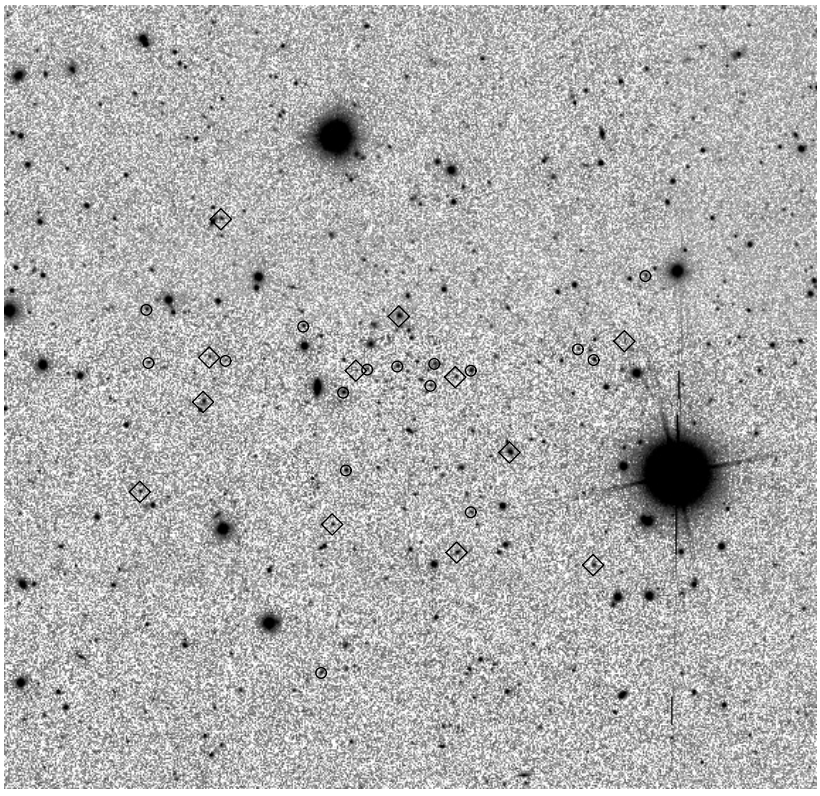

Fig. 5. A 10 × 10 arcmin cutout centered on the matched-filter position of EISJ2236-4017. Symbols follow those in Fig. 2, except that in this case only one significant groups is found. North is up, east to the left.

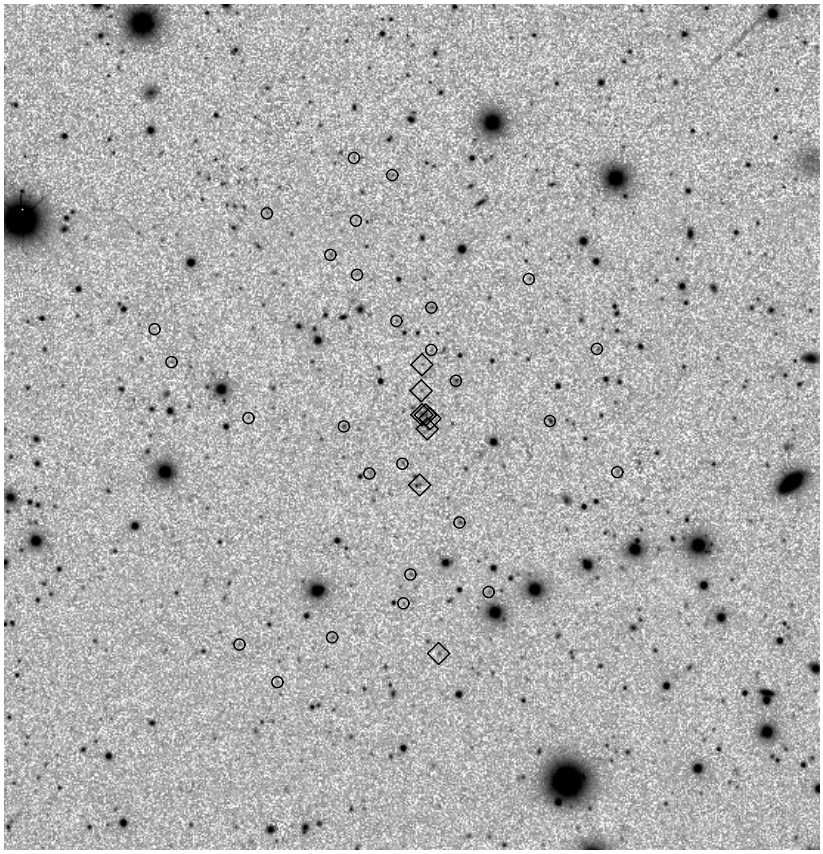

Fig. 6. A 10×10 arcmin cutout centered on the matched-filter position of EISJ2249-3958. Symbols follow those in Fig. 5. North is up, east to the left.

not all the masks were observed. In fact, the missing mask was the most likely to include the cluster brightest members in the central regions. This not only explains the significantly smaller number of galaxies with measured redshift, but the lack of visible clustering may also be due to the poor sampling achieved in this field. As can be seen from the image cutout the region around the matched-filter position at the center of the image is almost devoid of measured redshifts. It is thus likely that the concentration of galaxies in the center of the field corresponds to the matched-filter detection but does not have any measured redshifts.

Regardless of the match with the matched-filter detection there is evidence for the presence of a galaxy system at $z = 0.509$ with a velocity dispersion of 900 km s^{-1}.

4.5. EISJ2249-3958

In this field 35 redshifts were measured and are shown in the last row of Fig. 1. The distribution shows a distinct peak at $z \sim 0.7$ as well as other smaller peaks both in the foreground and background. Using the gap-technique, we indeed identify five groups with at least 3 members, but only one is significant according to the criteria adopted in this paper ($\sigma \geq 99\%$). As listed in Table 2 this cluster has a redshift of $z = 0.710$ ($\Delta z \sim -0.19$), somewhat smaller than that estimated by the matched filter, and a velocity dispersion of about 380 km s^{-1}, typical of groups. Inspection of the cone diagrams and the *I*-band image (Fig. 6) shows that seven out of eight confirmed member galaxies lie along an elongated structure extending only 2 arcmin. The remaining galaxy is positioned along the same axis but 2 arcmin away from the rest. The concentrated galaxies are the brightest ones found at the matched-filter position, and thus likely to correspond to the original detection. The small values of the velocity dispersion may be due to poor sampling or alternatively that this density enhancement is associated to a filament or a non-virialized cluster, instead of part of a relaxed system. However, deciding among these various possibilities must await further spectroscopic observations. For the time being, we consider the detected system in redshift space to correspond to the matched-filter detection of the projected distribution, which led to an overestimate of the redshift.

5. Discussion

The main objective of the present paper has been to extend the earlier work of Benoist et al. (2002) and present the results of a spectroscopic survey conducted at the VLT of the fields of 8 EIS candidate clusters with redshifts $z \geq 0.6$. From the above analysis we find that in three of the 5 fields considered here we identify two statistically significant density enhancements and one in each of the two remaining fields. More importantly, the measured redshifts for these systems range from $0.4 \lesssim z \lesssim 0.7$ and nearly all with velocity dispersions typical

Table 3. Summary of confirmed EIS clusters from this work and from Benoist et al. (2002).

Cluster	$z_{\rm MF}$	$z_{\rm spec}$	σ_v(km s^{-1})
EISJ0046-2930*	0.6	0.808	1170
EISJ0046-2951		0.614	1400
	0.9	0.671	865
EISJ0048-2942		0.402	1000
	0.6	0.638	1080
EISJ0050-2941		0.559	1375
		0.617	970
EISJ0533-2412*	1.3	1.301	–
EISJ0954-2023*		0.948	200
	1.1	1.141	290
EISJ2236-4017		0.509	900
EISJ2249-3958	0.9	0.710	380

* The spectroscopic confirmations of these systems were reported in Benoist et al. (2002).

of rich systems. A less obvious question is whether these detections are associated with the original matched-filter detection. In general, one would say yes but in at least one (but probably two) case(s) it appears that we have detected a foreground system and that detected by the matched-filter technique still needs to be confirmed by additional observations of fainter galaxies. Another point that must await further observations is the nature of the systems - namely, whether they form relaxed clusters, or are part of proto-clusters before infall, or density enhancements associated with filaments and walls. A preliminary effort in answering these questions is presented by Jørgensen et al. (2005, in preparation).

Combining the present results with those compiled by Benoist et al. (2002), our group has now studied the fields of 8 high-z candidate clusters, with all leading to at least one confirmed system. The properties of all the detected systems are listed in Table 3. The table gives: in Col. 1 the cluster field name; in Col. 2 the matched-filter estimated redshift, $z_{\rm MF}$, whenever we believe that there is a match between the detection in redshift and projected space; in Col. 3 the spectroscopic redshift, $z_{\rm spec}$, of the systems detected in redshift space; and in Col. 4 the estimated velocity dispersion of the system, σ_v.

For the six systems for which we believe to have identified the counterpart of the matched-filter detection we find that the difference between spectroscopic and estimated matched-filter redshifts range from $\Delta z = z_{\rm spec} - z_{\rm MF} = -0.229$ to $\Delta z = 0.208$, with a mean offset of $\Delta z = -0.022$ and a standard deviation of $\sim$0.15, therefore in excellent agreement with what would be expected from the estimated errors of the algorithm. This result is valid all the way to the highest redshifts found in the catalog and thus makes the EIS cluster candidate catalog a good source for drawing high-z clusters for more detailed studies.

6. Summary

In this paper we have presented the results of spectroscopic observations conducted with FORS1 at the VLT in the fields of 5 high-z ($z \geq 0.6$) cluster candidates identified by applying the matched-filter algorithm to the images from the EIS-WIDE I-band survey. The presence of galaxy clusters were supported by a color-slicing analysis targeting the individual detections. We find at least one significant system in all fields with redshifts in the range $0.40 < z < 0.71$ and from 8 to 33 confirmed cluster members. All systems, except one, have velocity dispersions $\gtrsim$800 km s^{-1} typical of that of rich clusters. Despite the intrinsic ambiguity of uniquely associating a significant density enhancement in redshift space with a detection in the projected distribution, the agreement of the matched filter and spectroscopic redshifts is, on average, excellent even though the matched filter has a tendency to overestimate them at higher redshifts. The results of this paper together with others of this series, strongly suggest that nearly all of the EIS candidate clusters identified applying the matched-filter algorithm to the I-band galaxy catalogs are associated with real density enhancements in redshift space regardless of the redshift domain. We conclude that the EIS Cluster Candidate Catalog is an excellent starting point to build a statistical sample of galaxy clusters at different redshifts for further investigation, complementing in many ways samples based on X-ray selection.

Acknowledgements. We would like to thank the referee for many useful comments, which helped improve the manuscript. LFO acknowledges financial support from the Carlsberg Foundation, the Danish Natural Sciences Research Council and the Poincaré fellowship program at Observatoire de la Côte d'Azur.

References

Benoist, C., da Costa, L., Olsen, L. F., et al. 1999, A&A, 346, 58
Benoist, C., da Costa, L., Jørgensen, H., et al. 2002, A&A, 394, 1
Gladders, M., López-Cruz, O., Yee, H., & Kodama, T. 1998, ApJ, 501, 571
Katgert, P., Mazure, A., Perea, J., et al. 1996, A&A, 310, 8
Kinney, A., Calzetti, D., Bohlin, R., et al. 1996, ApJ, 467, 38
Lilly, S., Fevre, O. L., Crampton, D., Hammer, F., & Tresse, L. 1995, ApJ, 455, 50
Nonino, M., Bertin, E., da Costa, L., et al. 1999, A&AS, 137, 51
Olsen, L., Hansen, L., Jørgensen, H., et al. 2003, A&A, 409, 439
Olsen, L., Benoist, C., da Costa, L., Hansen, L., & Jørgensen, H. 2005, A&A, 435, 781
Olsen, L. F. 2000, Ph.D. Thesis, Copenhagen University Observatory
Olsen, L. F., Scodeggio, M., da Costa, L., et al. 1999a, A&A, 345, 681
Olsen, L. F., Scodeggio, M., da Costa, L., et al. 1999b, A&A, 345, 363
Postman, M., Lubin, L., Gunn, J., et al. 1996, AJ, 111, 615
Ramella, M., Biviano, A., Boschin, W., et al. 2000, A&A, 360, 861
Scodeggio, M., Olsen, L. F., da Costa, L., et al. 1999, A&AS, 137, 83
Stanford, S., Eisenhardt, P., & Dickinson, M. 1998, ApJ, 492, 461

Online Material

Appendix A: Measured redshifts

Table A.1. The list of measured redshifts for the cluster EISJ0046-2951.

ID	$\alpha(J2000)$	$\delta(J2000)$	I	z
1	00:45:42.318	−29:48:14.68	20.52	0.8206
2	00:46:00.877	−29:49:27.56	21.93	0.6099
3	00:45:57.779	−29:49:30.50	21.51	0.6650
4	00:45:48.689	−29:49:39.00	21.47	0.6255
5	00:45:53.937	−29:49:51.54	19.92	0.6088
6	00:45:59.547	−29:50:30.09	21.22	0.7832
7	00:46:01.161	−29:51:35.91	21.46	0.3099
8	00:46:00.264	−29:52:29.38	18.59	0.2805
9	00:45:58.466	−29:52:40.12	21.10	0.8205
10	00:46:02.725	−29:53:55.33	21.46	0.7310
11	00:46:02.932	−29:53:55.28	22.60	0.7310
12	00:46:00.057	−29:53:58.11	21.40	0.7612
13	00:45:47.826	−29:47:38.91	20.67	0.2171
14	00:46:12.736	−29:47:41.42	21.92	0.6113
15	00:46:15.350	−29:47:43.35	21.77	0.6805
16	00:45:48.226	−29:47:54.55	20.89	0.6288
17	00:45:50.702	−29:48:02.36	20.19	0.4410
18	00:45:43.652	−29:48:14.77	20.69	0.8229
19	00:45:53.812	−29:48:13.45	21.17	0.4072
20	00:45:59.666	−29:48:19.38	21.66	0.4912
21	00:46:13.850	−29:48:19.92	21.22	0.2151
22	00:46:14.864	−29:48:24.76	20.24	0.5618
23	00:46:11.498	−29:48:24.65	20.74	0.1922
24	00:46:03.188	−29:49:11.56	18.20	0.6130
25	00:46:03.522	−29:49:08.03	19.34	0.6171
26	00:45:54.351	−29:48:51.43	20.75	0.6130
27	00:45:48.286	−29:48:51.89	21.37	0.2190
28	00:45:59.957	−29:49:02.26	20.78	0.6135
29	00:45:55.851	−29:49:06.60	20.61	0.5147
30	00:45:54.989	−29:49:04.22	20.60	0.5137
31	00:46:03.939	−29:49:08.80	20.06	0.1322
32	00:46:10.209	−29:49:06.74	21.19	0.6071
33	00:46:14.783	−29:49:08.51	20.97	0.5636
34	00:46:08.292	−29:49:13.98	19.58	0.6092
35	00:46:05.373	−29:49:16.20	21.74	0.6232
36	00:46:09.963	−29:49:14.78	21.88	0.3194
37	00:46:05.730	−29:49:16.89	20.93	0.1461
38	00:46:08.955	−29:49:18.13	21.22	0.6132
39	00:46:18.326	−29:49:24.38	21.95	0.3853
40	00:46:07.438	−29:49:35.66	21.62	0.4080
41	00:46:14.058	−29:49:38.96	21.48	0.6140
42	00:46:06.995	−29:49:42.90	22.07	0.7433
43	00:46:06.295	−29:49:54.80	20.10	0.6717
44	00:46:06.629	−29:49:54.86	20.74	0.5117
45	00:46:03.327	−29:50:12.70	19.71	0.4427
46	00:46:08.951	−29:50:15.14	21.73	0.8789
47	00:46:12.814	−29:50:33.70	20.51	0.6108
48	00:46:06.219	−29:50:39.72	21.72	0.5584
49	00:46:10.870	−29:51:06.54	19.96	0.7653
50	00:46:05.844	−29:51:07.94	19.94	0.5402
51	00:46:08.049	−29:51:09.97	21.85	0.6650
52	00:46:14.610	−29:51:13.81	20.48	0.6270
53	00:46:07.916	−29:51:24.57	19.75	0.6735
54	00:46:09.105	−29:51:25.28	21.86	0.6760
55	00:46:06.317	−29:51:27.77	21.02	0.6684
56	00:46:08.982	−29:51:30.55	21.92	0.3149
57	00:46:08.418	−29:51:37.73	20.59	0.2166
58	00:46:04.555	−29:52:53.72	21.04	0.5379
59	00:46:07.854	−29:53:22.11	21.93	0.6671
60	00:46:03.484	−29:53:24.55	22.01	0.2803
61	00:46:06.670	−29:53:24.75	21.20	0.5491
62	00:46:11.473	−29:51:40.39	20.95	0.6263
63	00:46:08.000	−29:51:41.17	21.33	0.6725
64	00:46:06.194	−29:51:36.85	22.28	0.4658
65	00:46:06.225	−29:51:55.60	21.29	0.7318
66	00:46:04.053	−29:51:50.77	21.83	0.7313
67	00:46:13.244	−29:51:50.10	21.29	0.7078
68	00:46:04.614	−29:52:16.66	21.81	1.1291
69	00:46:03.632	−29:52:20.23	21.72	0.7393
70	00:46:04.778	−29:52:44.59	22.00	0.3329
71	00:46:10.045	−29:53:09.80	21.09	0.6704

Table A.2. The list of measured redshifts for the cluster EISJ0048-2942.

ID	$\alpha(J2000)$	$\delta(J2000)$	I	z
1	00:48:30.904	−29:45:05.18	20.63	0.6400
2	00:48:31.854	−29:45:12.25	20.99	0.6307
3	00:48:28.238	−29:45:31.60	21.21	0.3765
4	00:48:22.606	−29:39:00.96	18.94	0.2015
5	00:48:21.332	−29:41:02.73	21.93	0.6447
6	00:48:20.495	−29:42:14.72	21.19	0.6350
7	00:48:22.138	−29:42:23.62	21.27	0.6973
8	00:48:20.672	−29:42:44.22	19.80	0.6086
9	00:48:24.625	−29:42:55.23	21.39	0.3528
10	00:48:18.750	−29:43:16.91	20.20	0.5421
11	00:48:19.632	−29:43:55.35	19.62	0.5398
12	00:48:21.985	−29:44:17.94	20.50	0.5418
13	00:48:20.124	−29:44:37.72	21.20	0.6252
14	00:48:37.912	−29:41:15.66	22.01	0.6426
15	00:48:31.682	−29:41:25.85	22.28	0.1319
16	00:48:26.160	−29:41:25.79	21.71	0.2119
17	00:48:29.152	−29:41:30.69	21.99	0.3293
18	00:48:32.630	−29:41:31.61	21.96	0.6508
19	00:48:40.353	−29:41:36.68	20.70	8.8888
20	00:48:29.387	−29:41:34.08	21.73	0.2251
21	00:48:35.571	−29:41:37.44	20.67	0.6355
22	00:48:34.576	−29:41:36.23	21.30	0.6332
23	00:48:39.006	−29:41:47.05	21.68	0.6412
24	00:48:41.578	−29:41:51.26	20.68	0.4411
25	00:48:26.023	−29:41:53.37	21.20	0.6994
26	00:48:37.715	−29:41:53.85	20.86	0.6383
27	00:48:41.216	−29:41:59.95	20.50	0.3989
28	00:48:37.907	−29:41:59.43	21.81	0.5175
29	00:48:32.699	−29:42:04.09	21.13	0.6375
30	00:48:42.141	−29:42:02.41	20.66	0.5476
31	00:48:31.883	−29:42:00.38	20.97	0.6393
32	00:48:29.181	−29:42:00.67	21.85	0.6390
33	00:48:31.385	−29:42:10.05	19.31	0.6409
34	00:48:29.308	−29:42:08.18	21.72	0.5476
35	00:48:30.050	−29:42:11.05	21.09	0.6495
36	00:48:42.060	−29:42:14.79	21.48	0.6351
37	00:48:27.635	−29:42:15.38	21.44	0.3962
38	00:48:39.379	−29:42:27.08	19.92	0.4600
39	00:48:29.671	−29:42:26.64	21.52	0.4363
40	00:48:35.710	−29:42:31.90	21.63	0.7419
41	00:48:34.754	−29:42:38.04	21.77	0.1975
42	00:48:35.763	−29:42:43.93	21.06	0.6506
43	00:48:40.461	−29:42:51.47	21.42	0.5476
44	00:48:30.271	−29:42:58.45	22.03	0.3786
45	00:48:43.648	−29:43:03.87	19.62	0.7632
46	00:48:33.060	−29:43:07.41	20.65	0.6319
47	00:48:38.103	−29:43:08.39	20.84	0.6379
48	00:48:30.788	−29:43:16.62	19.98	0.6357
49	00:48:40.006	−29:43:16.93	21.19	0.6369
50	00:48:42.113	−29:43:20.91	21.58	0.7665
51	00:48:41.507	−29:43:23.86	20.63	0.6987
52	00:48:37.402	−29:43:41.01	21.41	0.6319
53	00:48:41.557	−29:43:42.44	21.03	8.8888
54	00:48:37.266	−29:43:44.39	20.56	0.6370
55	00:48:26.997	−29:43:43.69	22.13	0.6790
56	00:48:31.317	−29:43:45.36	21.20	0.6275
57	00:48:39.264	−29:43:53.00	20.34	0.6423
58	00:48:38.473	−29:43:54.98	20.37	0.6754
59	00:48:37.685	−29:44:00.39	20.84	0.6352
60	00:48:35.311	−29:44:17.78	20.82	0.6364
61	00:48:31.112	−29:44:19.50	21.68	0.8626
62	00:48:40.986	−29:44:24.89	21.95	0.3015
63	00:48:33.184	−29:44:24.90	21.08	0.5002
64	00:48:28.204	−29:44:39.79	20.24	0.4082
65	00:48:31.408	−29:44:46.13	22.01	0.6301
66	00:48:30.987	−29:44:59.40	21.30	0.8240
67	00:48:30.116	−29:39:06.04	20.13	0.4043
68	00:48:27.736	−29:39:17.74	21.62	8.8888
69	00:48:33.042	−29:39:37.73	21.22	0.5217
70	00:48:39.234	−29:39:59.12	20.21	0.4011
71	00:48:41.374	−29:40:10.57	21.74	0.4743
72	00:48:27.598	−29:40:23.29	20.71	0.6379
73	00:48:40.952	−29:40:27.39	20.55	0.3967
74	00:48:44.138	−29:40:45.69	20.00	0.5312
75	00:48:36.816	−29:40:47.07	22.22	0.6350
76	00:48:36.927	−29:40:52.09	20.94	0.6328
77	00:48:29.378	−29:40:51.35	20.70	0.6450
78	00:48:48.161	−29:42:50.69	20.75	0.4071
79	00:48:46.908	−29:43:08.91	20.51	0.4604
80	00:48:47.426	−29:43:08.96	20.79	0.2197

Table A.2. continued.

Table A.3. The list of measured redshifts for the cluster EISJ0050-2941.

ID	$\alpha(J2000)$	$\delta(J2000)$	I	z
1	00:50:03.983	−29:41:19.24	21.54	0.3956
2	00:50:04.744	−29:41:20.27	21.67	0.5811
3	00:50:00.828	−29:41:24.02	20.74	0.8226
4	00:50:03.389	−29:41:40.52	21.97	0.6176
5	00:50:03.762	−29:42:33.94	21.00	0.5690
6	00:50:00.936	−29:42:39.07	21.98	0.5868
7	00:49:50.655	−29:42:49.86	22.00	0.5690
8	00:49:51.353	−29:42:50.19	21.43	0.5007
9	00:49:57.570	−29:43:04.84	19.36	0.5267
10	00:49:58.044	−29:42:58.77	21.81	0.1647
11	00:49:57.468	−29:43:08.72	21.43	0.5265
12	00:49:57.644	−29:43:43.54	22.04	0.5233
13	00:49:58.338	−29:43:57.60	21.12	0.5077
14	00:50:03.611	−29:37:39.81	21.48	0.3008
15	00:50:07.277	−29:37:36.06	21.31	0.3128
16	00:49:57.687	−29:38:17.10	20.65	0.5806
17	00:49:55.689	−29:38:35.31	19.98	0.5102
18	00:50:10.860	−29:38:32.40	21.06	0.4358
19	00:50:10.442	−29:39:00.98	20.17	0.5578
20	00:50:10.093	−29:39:08.55	19.96	0.5574
21	00:50:10.950	−29:39:22.25	22.10	0.5540
22	00:49:53.856	−29:39:26.65	20.18	0.7331
23	00:49:55.687	−29:39:34.21	20.01	0.6281
24	00:50:06.658	−29:39:35.57	21.38	0.7028
25	00:50:21.071	−29:39:37.27	21.21	0.6159
26	00:50:04.286	−29:39:39.02	21.27	0.6128
27	00:49:57.957	−29:39:41.95	21.30	0.5506
28	00:50:07.671	−29:39:48.92	20.37	0.6132
29	00:49:58.758	−29:40:11.11	21.70	0.6564
30	00:49:57.452	−29:40:02.42	21.36	0.5506
31	00:49:58.578	−29:40:10.92	22.71	0.6234
32	00:49:57.959	−29:40:28.87	20.57	0.5948
33	00:50:03.780	−29:40:48.08	20.45	0.6149
34	00:50:06.977	−29:40:47.66	21.50	0.5980
35	00:50:14.650	−29:40:52.39	20.69	0.6996
36	00:50:07.623	−29:40:49.35	21.92	0.4943
37	00:50:05.888	−29:40:56.94	21.80	0.2179
38	00:50:01.805	−29:40:57.71	20.97	0.3356
39	00:50:02.487	−29:40:58.06	22.01	0.3359
40	00:50:05.322	−29:41:03.77	22.04	0.3137
41	00:49:50.259	−29:41:07.57	21.76	0.4414
42	00:50:12.261	−29:41:16.64	22.07	0.5468
43	00:50:18.204	−29:41:26.93	20.83	0.5315
44	00:50:19.585	−29:41:33.25	19.11	0.6120
45	00:50:14.502	−29:41:39.32	20.70	0.5304
46	00:50:10.993	−29:41:43.32	21.25	0.7689
47	00:50:16.403	−29:41:53.57	21.46	0.4410
48	00:50:08.547	−29:42:03.15	21.62	0.4962
49	00:50:06.986	−29:42:11.97	21.07	0.5995
50	00:50:09.569	−29:42:22.78	20.41	0.3379
51	00:50:15.047	−29:43:05.89	20.29	0.3156
52	00:50:06.715	−29:43:36.08	20.84	0.5629
53	00:50:05.556	−29:44:00.26	20.18	0.5621
54	00:50:11.011	−29:44:22.21	21.17	0.5575
55	00:50:10.379	−29:44:40.59	21.12	0.5644

Table A.4. The list of measured redshifts for the cluster EISJ2236-4017.

ID	$\alpha(J2000)$	$\delta(J2000)$	I	z
1	22:36:23.524	−40:21:22.82	20.23	0.5727
2	22:36:02.714	−40:16:20.02	20.61	0.6503
3	22:36:18.851	−40:16:53.88	18.86	0.5062
4	22:36:04.007	−40:17:09.27	20.74	0.4988
5	22:36:07.049	−40:17:16.12	20.40	0.6250
6	22:36:06.005	−40:17:23.87	19.14	0.3308
7	22:36:16.462	−40:17:29.03	19.86	0.6248
8	22:36:14.059	−40:17:33.63	19.21	0.5969
9	22:36:18.895	−40:17:31.54	19.75	0.4471
10	22:36:20.863	−40:17:34.28	20.63	0.5571
11	22:36:21.606	−40:17:35.22	21.30	0.5089
12	22:36:15.069	−40:17:38.70	20.23	0.5126
13	22:36:16.693	−40:17:45.61	20.44	0.6455
14	22:36:22.419	−40:17:51.96	19.24	0.6256
15	22:36:11.417	−40:18:34.50	18.22	0.5139
16	22:36:22.142	−40:18:50.34	19.66	0.0751
17	22:36:13.885	−40:19:20.01	20.50	0.5680
18	22:36:22.978	−40:19:31.11	20.26	0.5095
19	22:36:14.760	−40:19:50.46	19.40	0.5143
20	22:36:05.780	−40:19:57.94	19.93	0.5097
21	22:36:30.651	−40:15:43.28	19.97	0.5143
22	22:36:35.441	−40:16:52.38	19.82	0.2381
23	22:36:25.117	−40:17:02.84	19.85	0.6462
24	22:36:31.255	−40:17:27.34	20.61	0.5061
25	22:36:30.178	−40:17:29.66	21.16	0.4262
26	22:36:35.239	−40:17:32.28	20.47	0.2026
27	22:36:31.602	−40:18:00.80	19.43	0.5039
28	22:36:35.651	−40:19:09.21	19.91	0.5070

Table A.5. The list of measured redshifts for the cluster EISJ2249-3958.

ID	$\alpha(J2000)$	$\delta(J2000)$	I	z
1	22:49:33.164	−39:59:56.62	21.70	0.3450
2	22:49:28.265	−40:00:10.34	21.59	0.6721
3	22:49:33.640	−40:00:17.34	22.12	0.5030
4	22:49:24.232	−40:00:34.68	21.77	8.8888
5	22:49:38.161	−40:00:40.94	21.55	0.2749
6	22:49:31.482	−40:00:54.10	21.43	0.7061
7	22:49:25.362	−39:55:42.70	21.22	8.8888
8	22:49:37.812	−39:56:04.71	21.36	0.7471
9	22:49:24.025	−39:56:11.05	21.57	8.8888
10	22:49:36.162	−39:56:19.42	21.86	0.7245
11	22:49:25.378	−39:56:24.84	21.82	0.5027
12	22:49:31.537	−39:56:44.18	20.98	0.6568
13	22:49:33.746	−39:56:53.37	21.77	0.4274
14	22:49:48.942	−39:56:55.95	22.49	1.0059
15	22:49:21.179	−39:57:16.22	21.29	0.5286
16	22:49:31.593	−39:57:14.72	21.97	0.5681
17	22:49:47.923	−39:57:19.96	21.49	0.7468
18	22:49:32.189	−39:57:25.29	21.68	0.7103
19	22:49:30.078	−39:57:37.36	20.29	0.5698
20	22:49:32.265	−39:57:44.10	21.82	0.7108
21	22:49:32.247	−39:58:01.47	19.80	0.7127
22	22:49:31.747	−39:58:04.26	21.40	0.7088
23	22:49:32.028	−39:58:01.61	20.83	0.7075
24	22:49:24.222	−39:58:07.66	19.97	0.5260
25	22:49:43.154	−39:58:01.43	22.10	0.7286
26	22:49:23.216	−39:58:07.41	21.16	8.8888
27	22:49:31.932	−39:58:11.74	20.53	0.7093
28	22:49:37.168	−39:58:08.80	20.84	0.8453
29	22:49:33.538	−39:58:36.52	21.11	0.5555
30	22:49:35.627	−39:58:43.12	22.24	0.9299
31	22:49:20.042	−39:58:45.46	21.65	0.5012
32	22:49:43.364	−39:58:48.64	22.01	8.8888
33	22:49:32.475	−39:58:52.08	21.06	0.7122
34	22:49:35.232	−39:58:55.16	21.64	8.8888
35	22:49:30.020	−39:59:19.77	20.82	0.5557
36	22:49:43.991	−40:00:44.86	22.30	0.7470
37	22:49:41.654	−40:01:12.55	21.97	0.9072
38	22:49:36.215	−39:54:55.04	21.75	0.7277
39	22:49:33.834	−39:55:07.99	21.69	0.4917
40	22:49:36.168	−39:55:40.36	22.20	0.6173
41	22:49:41.750	−39:55:33.83	22.25	0.5281
42	22:49:40.305	−39:55:14.17	22.21	8.8888